Article

High-Throughput Canopy and Belowground Phenotyping of a Set of Peanut CSSLs Detects Lines with Increased Pod Weight and Foliar Disease Tolerance

Davis Gimode [1,2], Ye Chu [1], Corley C. Holbrook [3], Daniel Fonceka [4], Wesley Porter [5], Iliyana Dobreva [6], Brody Teare [7], Henry Ruiz-Guzman [7], Dirk Hays [7,8] and Peggy Ozias-Akins [1,*]

1   Institute of Plant Breeding Genetics and Genomics, University of Georgia, Tifton, GA 31793, USA; dgimode@gmail.com (D.G.); ychu@uga.edu (Y.C.)
2   International Crops Research Institute for the Semi-Arid Tropics, Nairobi P.O. Box 39063-00623, Kenya
3   United States Department of Agriculture, Agricultural Research Service, Tifton, GA 31793, USA; corley.holbrook@ars.usda.gov
4   Centre d'Etude Régional pour l'Amélioration de l'Adaptation à la Sécheresse (CERAAS), Institut Sénégalais de Recherches Agricoles (ISRA), BP 3320, Route de Khombole, Thiès 21000, Senegal; daniel.fonceka@cirad.fr
5   Crop and Soil Sciences Department, University of Georgia, Tifton, GA 31793, USA; wporter@uga.edu
6   Department of Geography, The Ohio State University, Colombus, OH 43210, USA; dobreva.iliyana.phd@gmail.com
7   Molecular & Environmental Plant Sciences, Texas A&M University, College Station, TX 77843, USA; blteare@gmail.com (B.T.); henry.ruiz@tamu.edu (H.R.-G.); dirk.hays@ag.tamu.edu (D.H.)
8   Department of Soil and Crop Sciences, Texas A&M University, College Station, TX 77843, USA
*   Correspondence: pozias@uga.edu

Abstract: We deployed field-based high-throughput phenotyping (HTP) techniques to acquire trait data for a subset of a peanut chromosome segment substitution line (CSSL) population. Sensors mounted on an unmanned aerial vehicle (UAV) were used to derive various vegetative indices as well as canopy temperatures. A combination of aerial imaging and manual scoring showed that CSSL 100, CSSL 84, CSSL 111, and CSSL 15 had remarkably low tomato spotted wilt virus (TSWV) incidence, a devastating disease in South Georgia, USA. The four lines also performed well under leaf spot pressure. The vegetative indices showed strong correlations of up to 0.94 with visual disease scores, indicating that aerial phenotyping is a reliable way of selecting under disease pressure. Since the yield components of peanut are below the soil surface, we deployed ground penetrating radar (GPR) technology to detect pods non-destructively. Moderate correlations of up to 0.5 between pod weight and data acquired from GPR signals were observed. Both the manually acquired pod data and GPR variables highlighted the three lines, CSSL 84, CSSL 100, and CSSL 111, as the best-performing lines, with pod weights comparable to the cultivated check Tifguard. Through the combined application of manual and HTP techniques, this study reinforces the premise that chromosome segments from peanut wild relatives may be a potential source of valuable agronomic traits.

Keywords: peanut; phenomics; high-throughput phenotyping; ground penetrating radar; tomato spotted wilt virus; leaf spot; pod weight

1. Introduction

A key challenge in peanut breeding is increasing the genetic diversity of the crop. Unlike their wild relatives, cultivated varieties have severely limited variation as a result of their genetic heritage and the process of domestication [1]. What is now recognized as cultivated peanut arose from the hybridization of two wild species, namely *A. duranensis* and *A. ipaensis*. Spontaneous doubling of the chromosomes of the hybrid resulted in tetraploid *A. hypogaea* [2,3]. The resultant ploidy barrier restricted the ability of cultivated peanut to exchange genetic material with the wilds. This limitation was further enforced

by the process of human selection and domestication [4,5]. Consequently, peanuts are under the constant threat of biotic pressures, such as insects and diseases, as well as abiotic stresses, such as drought, which are exacerbated by the effects of climate change. In contrast, because of their diversity, wild peanut relatives are more adaptable since they have maintained genes that enable them to cope with these pressures. This makes them precious sources of diversity for cultivated peanut [6–9].

One of the ways that breeders sought to harness genetic diversity from the wild was by creating a chromosome segment substitution line (CSSL) population [1]. This was achieved by crossing the two known diploid ancestors of peanut to result in a diploid hybrid. The genome of the hybrid was doubled to form a synthetic tetraploid, essentially recreating the allotetraploid ancestor of cultivated peanut [10]. The synthetic allotetraploid was crossed with Fleur 11, a cultivated variety of peanut that is popularly grown in West Africa. Subsequent judicious selection resulted in a population comprised of 122 individual lines. Each line is genetically similar to the cultivated variety; however, the selection was made such that each line retained a small segment of the synthetic genome. Therefore, each line is distinguished by the portion of the synthetic genome it contains, while at the same time, the whole genome of the wild tetraploid is captured in the entire population [1]. The CSSL population, thus, constitutes a critical peanut genetic resource, with the potential to enable understanding of the basis of genetic variation in peanut.

High-resolution genetic characterization of wild introgressions in this population has been achieved previously, made possible by taking advantage of technological improvements and reduced costs, which have made it easier to obtain genotype data. These factors have enabled peanut researchers to achieve the phenomenal feat of releasing high-quality whole genome sequences of the tetraploid species [11], as well as the A and B genome progenitors of cultivated peanut [12]. Other genetic resources, including two high-quality SNP arrays [13–16], a reference transcriptome [17] as well as a comprehensive genomics database [18], have ensured the graduation of peanut from an orphan crop status [19].

Despite the ease of access and routine deployment of high-throughput genotyping, peanut phenotyping is mostly carried out at low throughput. Typically, this involves studying single plants in controlled environments such as greenhouses and growth chambers, or in small field plots for traits such as disease resistance. At the same time, it is often necessary to harvest plants destructively and at fixed growth stages. Greenhouse and growth chamber conditions fail to capture the true attributes of the plants since, when they are grown in the field, they behave differently at the various growth stages and as a result of competition for water, nutrients, and sunlight [20–22]. Additional drawbacks of such manual phenotyping include the fact that it is time-consuming, labor and cost intensive, and prone to human error and biases. This phenotyping challenge forms a bottleneck in the peanut breeding pipeline that curtails the full exploitation of available genetic and genomic resources for association studies.

A practical way of alleviating this bottleneck is the use of phenomics, or high-throughput phenotyping (HTP), a novel approach that is increasingly finding application in plant breeding research. It combines cutting-edge technologies such as spectroscopy, noninvasive imaging, and high-performance computing to capture phenotypic data at high resolution and throughput to address breeding problems [22]. HTP involves the use of equipment that can facilitate the collection of large quantities of high-quality data in a short period, thus availing the possibility of linking genotype data with phenotype data of equal throughput obtained in a "real world" environment. Field-based HTP, in particular, enables the accurate measurement of plant growth, architecture, and performance non-destructively and in the complexity of their true environment [22–24]. Such phenomic approaches can facilitate the effective use of genetic data to discover novel variations that could improve the quality and yield of crops [25].

Two commonly used field HTP techniques in studying crop plants involve remote sensing using visible light cameras (RGB) and multispectral cameras. These are typically borne on unmanned aerial vehicles (UAV) and can be useful for evaluating plant biotic

and abiotic stress, plant vigor and phenology, soil characterization, and field mapping [26]. Examples of studies utilizing such techniques include studying the response to nitrogen and fertilizer treatment in maize [27,28], evaluation of water and nitrogen use efficiency in rice [29,30], and evaluation of pest pressure and yield estimation in soybean [31,32].

In peanut, UAV-based remote sensing has been used to acquire data on NDVI, canopy temperature, and RGB images to discriminate between various varieties based on yield under drought and late leaf spot pressure [33,34]. An attempt was made to derive canopy spectral signatures for predicting pod maturity, though without significant success [35]. Patrick et al. [36] experimented with various multispectral indices to determine the best one for detecting TSWV and settled on NDRE, which detected TSWV as early as 93 days into the season. Sarkar et al. [37] used a digital camera mounted on a UAV to successfully evaluate leaf wilting for irrigation triggering using indices derived from red–blue–green images. Manual and UAV-based HTP were compared for their utility to assess key traits in the US mini-core collection by Sarkar et al. [38]. The study showed good correlations between NDVI and RGB indices with traits such as plant height, lateral growth, leaf wilting, thrips damage, and yield, suggesting that vegetative indices could be used as surrogates for trait selection. Bagherian et al. [39] combined the use of aerial hyperspectral imaging with machine learning to predict biomass, pod count, and yield. Correlations of up to 0.73 were observed between measured biomass and its prediction.

Of equal novelty is the use of ground penetrating radar (GPR) for belowground studies. GPR works by emitting electromagnetic waves into the ground and detecting the waves that are reflected back to a detector. This enables the detection and rendering of 3D images of belowground biomass [40]. GPR has been effectively used for the non-destructive study of belowground biomass, especially for trees under various soil conditions [41], in forest systems [42], tree intercropping systems [43], and other agroforestry systems [44,45]. However, its application in studying fine belowground biomass, characteristic of agricultural crops, has been limited [46].

Most studies of the application of GPR to belowground phenotyping have used image analysis and image-thresholding analysis to extract GPR features, which are then correlated to crop characteristics such as biomass [40,46]. Dobreva et al. [47] demonstrated the limitations of this approach for the assessment of peanut yield. Specifically, it was demonstrated that the information about peanut yield is located within narrow vertical strips of the radargram. Moreover, due to the sensitivity of the GPR signal to soil heterogeneity, applying the same approach to a different geographic site or even to the same geographic site with different soil moisture conditions results in a different depth from which maximum peanut information can be detected. A frequency-based approach to agricultural GPR involves transforming the radar information from the time to the frequency domain. Agbona et al. [48] demonstrated the application of Fourier transform to belowground phenotyping of cassava. The advantage of this implementation is that a larger vertical portion of the radargram can be analyzed, which eliminates the need to determine the narrow vertical location of maximum peanut yield if image thresholding is applied. It is also expected that this approach is less sensitive to the specific soil conditions of different geographic sites. Peanut is a geocarpic plant that flowers aboveground but sets seed belowground [49], and, therefore, the most important biomass of peanut is below the ground. Consequently, the phenotyping of peanut pods requires a destructive harvest. This makes peanut an important candidate for the development of non-destructive belowground phenotyping techniques such as GPR.

Thus, the peanut CSSL population was an ideal candidate for deploying HTP techniques to bridge the genotype-phenotype gap. In this study, we incorporated HTP into the screening of a subset of the CSSLs that exhibited contrasting morphological attributes for canopy and belowground traits. Initially, the objective was to capture morphological diversity inherent in the population as a result of the differences in their genetic composition. However, as serendipity would have it, increased tomato spotted wilt disease and leaf spot pressure afforded the opportunity to evaluate the performance of the lines under

disease pressure. Aerial images were collected and correlated with manual disease ratings. In addition, GPR was used to evaluate pod weight prior to harvest.

2. Materials and Methods

A subset of 26 lines from a CSSL population originally developed by [1] was used for this study. In addition, Fleur 11, the cultivated parent, as well as Tifguard and Florunner, which are morphologically distinct from the CSSLs, were also planted as adapted high-yielding leaf spot and TSWV-resistant checks for a total number of 29 lines. Two field trials were conducted with the lines planted in May 2018 at the University of Georgia Tifton Campus' Bowen and Gibbs farms, with the soil type being Tift loamy sand (fine-loamy, kaolinitic, thermic Plinthic Kandiudults). The experimental setup in each field was RCBD, with three replicates in each field except for CSSL 15, which had 2 replicates in both fields, and CSSL 100, which had 2 replicates at Gibbs due to seed shortage. Each 3 m long plot had two rows with the seeds sown with a spacing of 7 cm between seeds. Normal cultural practices, including scheduled pesticide and fungicide application and irrigation, were followed. Ratings for mid-season TSWV were recorded at approximately 80 days after planting (DAP) for both fields, as well as RGB and thermal aerial imaging. At the end of the season (110 DAP), ratings for leaf spot were carried out on both fields, while TSWV was rated on the Gibbs farm only. For TSWV, the ratings entailed assessing canopy TSWV symptoms on a scale of 0 to 10, with 0 being no symptoms observed and 10 being the presence of symptoms in the entire plot. An immunostrip assay was carried out to confirm the presence of TSWV in susceptible lines and its absence in lines that were asymptomatic. Leaf spot ratings were carried out without making a distinction between early and late leaf spot on a scale of 1, indicating no leaf spot symptoms, to 10, indicating complete defoliation and plant death. Thermal and multispectral images were collected on the same day that TSWV rating was undertaken. All cameras used for aerial imaging were mounted on a 3 DR Solo quadcopter.

GPR data were collected at 117 DAP, which was 1 day before plot inversion. The GPR imaging system was an experimental prototype consisting of an array of 7 antennas developed by IDS GeoRadar systems. Both rows in each of the 85 plots were scanned at Gibbs farm; however, only 49 of the 86 plots had both rows scanned at Bowen, with the rest having only single rows scanned. Post-harvest, manual data was collected by taking the total pod weight of each plot.

Analysis

Indices derived from RGB images were the Visible Atmospherically Resistant Index (VARI), Green Vegetation Index-R (GRV), and Green Leaf Index (GLI). Multispectral indices were the Chlorophyll Index-RE (CIRE), Difference Vegetation Index (DVI), Green Normalized Difference Vegetation Index (GNDVI), Normalized Difference Vegetation Index (NDVI), Normalized Green (NG), Optimized Soil Adjusted Vegetation Index (OSAVI), Ratio Vegetation Index (RVI), Soil Adjusted Vegetation Index (SAVI), and Triangular Vegetation Index (TVI). Canopy temperature depression (CTD, a measure of the temperature difference between the canopy and the surrounding area) was derived from the thermal images. Collected images were stitched using the photogrammetry software Pix4D (Prilly, Switzerland) and resulted in whole-field orthomosaics. ArcGIS [50] was used for further downstream analysis. Briefly, the various indices were calculated to extract data from the RGB, multispectral, and thermal orthomosaics. Boundaries were manually drawn to delineate each plot in the fields with appropriate buffering to ensure no overlap between plots. Pixels outside the plot boundaries were eliminated. Within the plots, thresholds of pixels representing soil were manually determined using the identity function and eliminated. Canopy pixels were averaged to derive quantitative data for each line. CTDs were calculated by subtracting the average plot temperature value from the air temperature which was obtained for each field from the University of Georgia Weather Network (www.weather.uga.edu, accessed on 20 March 2023).

GPR data were processed using the Python software platform GPR-Studio (Hays, pers. Comm.). Data from channel 3 were used for downstream signal processing. To begin with, the radargrams were split into plots based on electronic markers that had been incorporated into the images at the time of GPR acquisition. In an ideal HTP setting, the radargrams should be split into plots using the electronic markers alone, but in this study, each agricultural plot was examined manually, and the markers adjusted to ensure that all plots were of the same length. The radargrams were also subset vertically to remove the top and bottom portions of the radargram. Specifically, the analysis was performed on the portion of the radargram that started at pixel row 160 and for a depth of 200 pixel rows.

Three GPR processing pipelines were tested. In the first pipeline, no processing was applied other than the vertical subset of the radargram. In the second and third pipelines, subset radargrams were filtered with Kirchoff migration and a migration window of 5 and 35, respectively. Migration focuses the signal, and a migration window refers to the width around each sample that is used to perform the migration, with a small window corresponding to a smaller effect of the migration. The output of the three pipelines was subjected to discrete Fourier transformation (DFT), and similar to Agbona et al. [48], the results of the DFT were averaged for each agricultural plot. Raw data following processing with the three pipelines and application of DFT are available in Tables S1–S3. The GPR features were derived from the power of the Fourier coefficients for specific frequency bins. The features were within the frequency ranges of 1–13, with each frequency delineated to 7 sub-frequencies (such that frequency 1 contained sub-frequencies 1, 1.143, 1.286, 1.429, 1.571,1.714, and 1.857, and so on) for a total of 91 features per single row scanned. The 7 sub-frequencies were combined to derive one variable per frequency by a trapezoidal approximation of the area under the sub-frequency curve (AUFC) using the formula:

$$AUFC = \sum_{i=1}^{n-1} \frac{d_i + d_{i+1}}{2} \times (s_{i+1} - s_i) \tag{1}$$

where d_i is the value of DFT at the ith observation, s_i is sub-frequency at the ith observation, and n is the total number of observations. The AUFC variables were regarded as the quantitative data points representing belowground pod variation for the population. The variables were labeled by prefixing the pipeline and suffixing the frequency from which it was derived; for example, p1_freq_1 was the variable for the first frequency of pipeline 1. Thirteen variables were derived for each pipeline to yield a total 39 quantitative GPR variables.

All aerial, belowground, and manual quantitative data were analyzed using R [51]. The partitioning of variance was carried out using mixed model linear regression with the lmerTest package [52] in R with FDR used for multiple hypothesis correction. Trait summaries and correlations were derived from the obtained coefficients. Where appropriate, broad sense heritability was obtained by calculating the ratio of genetic variance to the total variance. For statistically significant traits ($p < 0.05$), lines that were significantly different from Fleur 11 ($p < 0.05$) were determined by running a Dunnett's multiple comparison test [53]. The relative effects of introgression on the traits were calculated by taking the difference between the coefficients of each line and Fleur 11 and getting the percentage relative to Fleur 11 ((CSSL−Fleur 11)/Fleur 11) × 100). Pearson correlation was used to investigate the relationship between the HTP data and the appropriate manual data.

3. Results

3.1. Manual Phenotyping

Ratings for TSWV were produced in the middle and at the end of the season. Due to more severe leaf spot incidence at the Bowen farm, it was not possible to accurately collect TSWV data at the end of the season. For mid-season TSWV, there were significant differences among the lines with no interaction between the fields. Late-season ratings at the Gibbs farm also revealed significant differences between the lines (Tables 1 and S4).

The line with the best rating mid-season was CSSL 100, which outperformed the cultivated check Tifguard. CSSL 111 was ranked third, while Fleur 11 ranked last (Table 2). End-season data from Gibbs showed that CSSL 100 was still the best-ranked within the population; however, Tifguard outperformed it (Figure 1 and Table 2). Overall, the best-performing CSSL lines under TSWV pressure were CSSL 100, CSSL 84, CSSL 15, and CSSL 111.

Table 1. Summary statistics for manually collected traits and spectral indices for the chromosome segment substitution line (CSSL) population.

Name [a]	Field	Significance	Mean	Min	Max	Fleur 11	SE [b]	Heritability [c]
Leaf spot late-season	Bowen	***	5.39	2.55	7.33	6.17	0.273	0.64
Leaf spot late-season	Gibbs	***	5.00	3.00	7.00	6.36	0.212	0.57
TSWV mid-season	Bowen	***	2.11	−0.12	4.67	4.67	0.243	0.57
TSWV mid-season	Gibbs	***	2.89	0.67	5.33	5.00	0.219	0.40
TSWV late-season	Gibbs	***	4.98	1.00	8.17	5.67	0.354	0.48
Pod weight (g)	Bowen	***	688.64	414.00	1320.00	498.00	45.189	0.54
Pod weight (g)	Gibbs	***	898.82	540.67	1610.00	705.33	44.817	0.74
GLI	Bowen	***	0.17	0.14	0.19	0.14	0.002	0.37
GLI	Gibbs	***	0.18	0.15	0.20	0.15	0.002	0.74
GRV	Bowen	***	0.13	0.11	0.16	0.11	0.003	0.56
GRV	Gibbs	***	0.15	0.13	0.16	0.13	0.002	0.70
VARI	Bowen	***	0.19	0.16	0.26	0.16	0.006	0.72
VARI	Gibbs	***	0.22	0.19	0.28	0.20	0.004	0.76
Mid CTD	Bowen	NS	−9.29	−10.62	−8.37	−9.74	0.076	0.00
Mid CTD	Gibbs	NS	−10.79	−11.53	−10.10	−11.28	0.076	0.03
End CTD	Bowen	***	−9.14	−11.01	−6.76	−10.30	0.178	0.22
End CTD	Gibbs	***	−10.31	−11.36	−9.01	−10.91	0.093	0.25
CIRE	Bowen	***	−0.56	−0.73	−0.47	−0.48	0.015	0.55
CIRE	Gibbs	***	−0.59	−0.70	−0.46	−0.48	0.012	0.69
DVI	Bowen	***	0.31	0.22	0.45	0.23	0.013	0.64
DVI	Gibbs	***	0.35	0.27	0.43	0.28	0.008	0.65
GNDVI	Bowen	***	0.70	0.62	0.82	0.66	0.010	0.78
GNDVI	Gibbs	***	0.73	0.68	0.81	0.69	0.006	0.62
NDVI	Bowen	***	0.71	0.59	0.86	0.63	0.014	0.66
NDVI	Gibbs	***	0.76	0.67	0.84	0.69	0.008	0.64
NG	Bowen	***	0.13	0.08	0.15	0.14	0.004	0.76
NG	Gibbs	***	0.12	0.09	0.14	0.13	0.002	0.66
OSAVI	Bowen	***	0.60	0.47	0.76	0.50	0.015	0.65
OSAVI	Gibbs	***	0.65	0.55	0.74	0.57	0.009	0.64
RVI	Bowen	***	7.37	4.05	14.88	4.62	0.579	0.76
RVI	Gibbs	***	8.72	5.63	13.26	6.04	0.384	0.73
SAVI	Bowen	***	0.49	0.37	0.65	0.40	0.016	0.64

Table 1. *Cont.*

Name [a]	Field	Significance	Mean	Min	Max	Fleur 11	SE [b]	Heritability [c]
SAVI	Gibbs	***	0.54	0.44	0.63	0.46	0.009	0.65
TVI	Bowen	***	18.62	13.08	27.34	13.73	0.814	0.61
TVI	Gibbs	***	21.33	15.94	25.99	16.84	0.504	0.65

NS: $p > 0.05$; *** $p \leq 0.001$. [a] Abbreviations for names: TSWV—tomato spotted wilt virus, GLI—Green Leaf Index, GRV—Green Vegetation Index-Red, VARI—Visible Atmospherically Resistant Index, CTD—canopy temperature depression, CIRE—Chlorophyll Index-Red Edge, DVI—Difference Vegetation Index, GNDVI—Green Normalized Difference Vegetation Index, NDVI—Normalized Difference Vegetation Index, NG—normalized green, OSAVI—Optimized Soil Adjusted Vegetation Index, RVI—Ratio Vegetation Index, SAVI—Soil Adjusted Vegetation Index, TVI—Triangular Vegetation Index; [b] standard error; [c] broad-sense heritability.

Table 2. Rankings for the chromosome segment substitution lines (CSSLs) based on manually collected data for both Bowen and Gibbs fields.

| Sample	TSWV (MS)	Rank TSWV (MS)	TSWV (LS)	Rank TSWV (LS)	Leaf Spot	Rank Leaf Spot	Pod Weight (g)	Rank Pod Weight
CSSL 009	4.67	28	7.33	27	6.00	19	681.67	22
CSSL 010	3.50	21	8.17	29	6.17	20	705.67	18
CSSL 013	3.17	18	6.50	24	6.42	24	805.33	7
CSSL 014	2.67	13	6.33	22	5.25	9	747.67	9
CSSL 015	1.26	4	3.50	6	4.25	6	589.83	27
CSSL 022	3.83	27	7.83	28	6.42	25	732.00	11
CSSL 025	3.50	23	5.67	16	6.67	27	702.67	19
CSSL 027	3.67	26	6.67	25	6.50	26	681.67	21
CSSL 031	2.17	8	4.00	7	5.67	13	696.00	20
CSSL 044	2.33	12	4.83	11	5.83	15	713.33	16
CSSL 051	2.17	9	5.00	13	5.83	16	717.67	15
CSSL 053	3.00	16	4.50	9	5.75	14	512.67	29
CSSL 055	2.33	10	4.33	8	5.00	7	547.33	28
CSSL 056	3.67	25	4.67	10	6.25	22	666.33	23
CSSL 058	3.33	20	6.17	19	6.83	28	725.33	13
CSSL 060	2.33	11	6.17	18	5.33	11	828.33	6
CSSL 061	3.17	19	7.00	26	6.92	29	709.00	17
CSSL 062	2.83	14	5.33	14	5.92	18	661.33	24
CSSL 069	3.67	24	6.17	20	5.25	10	832.33	5
CSSL 084	1.33	5	3.17	4	4.17	5	1465.00	1
CSSL 100	0.41	1	2.00	2	3.33	2	994.10	4
CSSL 111	1.00	3	3.50	5	3.75	3	1299.33	2
CSSL 112	3.00	15	4.83	12	5.58	12	728.00	12
CSSL 113	3.17	17	6.50	23	5.83	17	722.33	14
CSSL 115	1.67	6	6.33	21	5.17	8	743.67	10
CSSL 121	3.50	22	5.67	15	6.17	21	645.67	25
Fleur 11	4.83	29	5.67	17	6.25	23	601.67	26
Florunner	1.83	7	2.67	3	3.83	4	802.00	8
Tifguard	0.50	2	1.00	1	3.25	1	1014.67	3

MS: mid-season; LS: late-season.
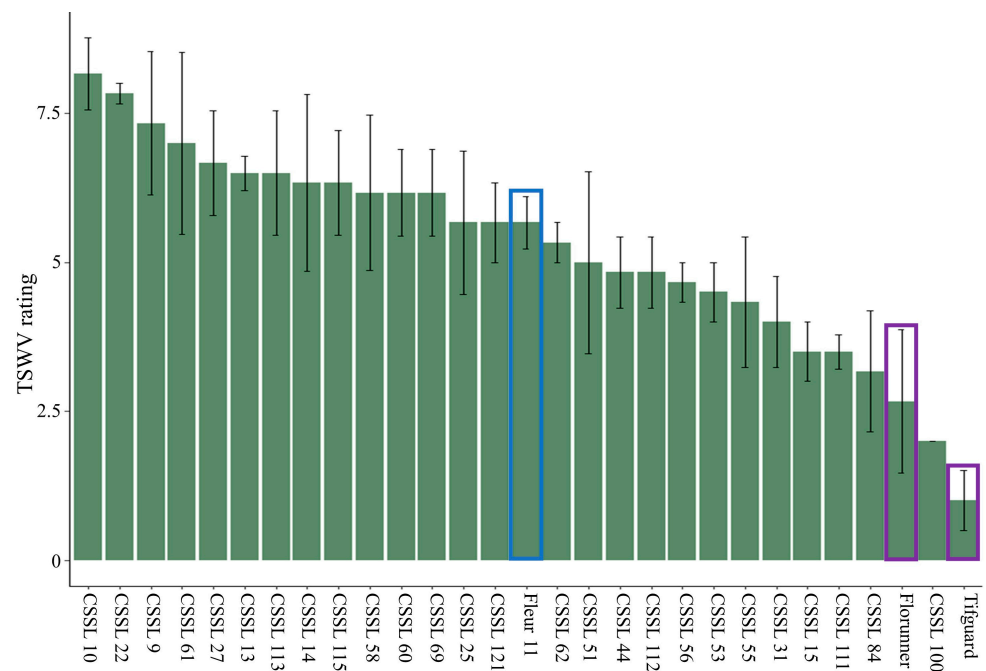
Figure 1. Manually collected end-season tomato spotted wilt virus (TSWV) scores for the chromosome segment substitution lines (CSSLs) showing multiple lines with a lower disease rating than Fleur 11, highlighted in blue. Adapted checks are highlighted in purple. The data were collected at Gibbs farm at 110 DAP.

Leaf spot was rated at the end of the season at both Gibbs and Bowen farms. The data revealed significant differences among the lines with no interaction between the fields (Tables 1 and S4). Overall, the best lines were CSSL 100 and CSSL 111, which were just below Tifguard, while CSSL 84 and CSSL 15 were third and fourth and ranked below the other check variety, Florunner (Figure 2 and Table 2).
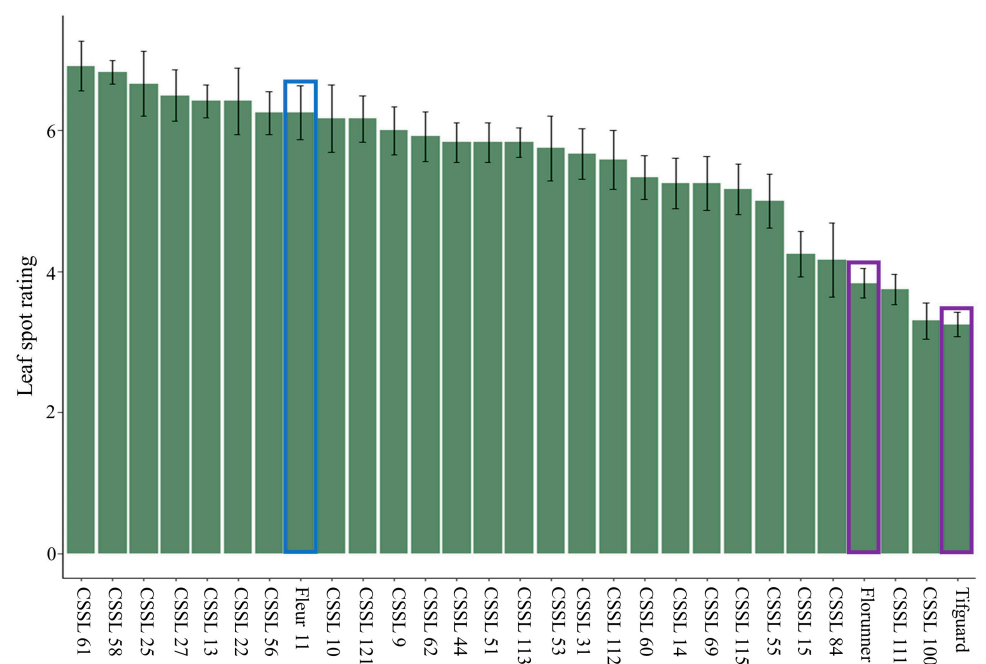

Figure 2. Manual leaf spot scores for the chromosome segment substitution lines (CSSLs) showing multiple lines with a lower disease rating than Fleur 11, highlighted in blue. Adapted checks are highlighted in purple. The data were collected from both Gibbs and Bowen farms at 110 DAP.

Pod weight data showed significant differences between the lines with some interaction between the fields (Tables 1 and S4). Overall, the best lines were CSSL 84 and CSSL 111, which performed better than the checks. CSSL 100 was the third best, ranking just below Tifguard (Figure 3 and Table 2). From Gibbs, the order of the top-ranked lines was CSSL 84, CSSL 111, and CSSL 100, followed in the fourth rank by Tifguard. At Bowen, CSSL 84 and CSSL 111 were at the top, followed by Florunner and Tifguard, with CSSL 100 falling to the seventh rank (Table S5). This could be attributed to the fewer number of seeds available for planting that resulted in two reps planted at Bowen for CSSL 100. Comparison of introgression lines showed consistently superior performance of CSSL 84 and CSSL 111 in both fields, with CSSL 100 being significantly different from Fleur 11 only at Gibbs. The analysis also highlighted CSSL 69 as having a superior pod weight relative to Fleur 11, but only at Gibbs (Table S6).
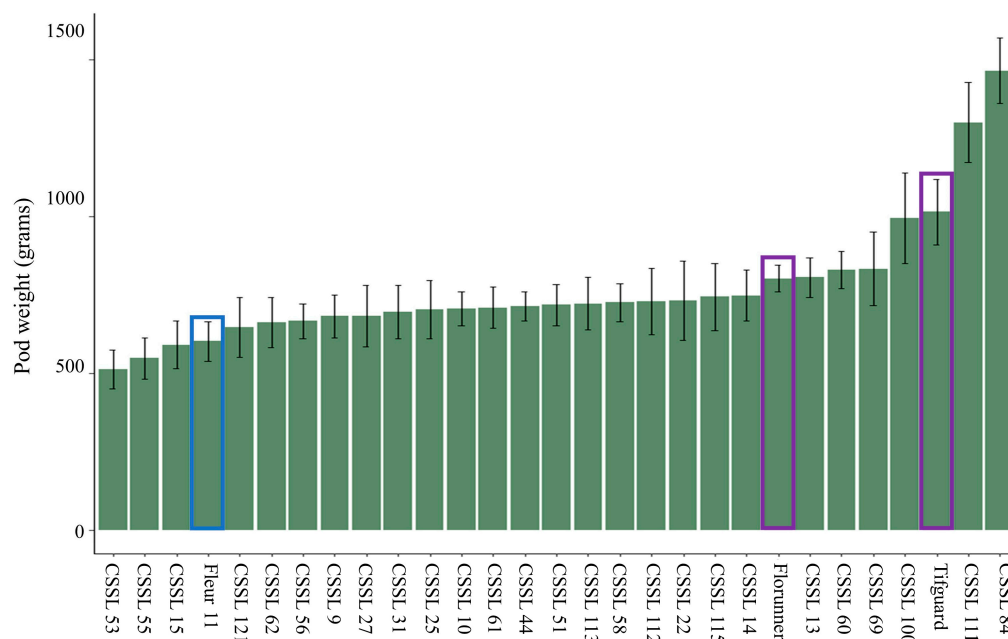

Figure 3. Pod weight for the chromosome segment substitution lines (CSSLs) showing multiple lines with a superior performance relative to Fleur 11, highlighted in blue. Adapted checks are highlighted in purple. The data were collected from both Gibbs and Bowen farms after harvest.

3.2. Aerial Phenotyping

A total of 14 traits that included 3 RGB indices, 9 multispectral indices and 2 canopy temperature traits were derived from aerial images. RGB images were acquired in the middle of the season, and the derived indices showed significant differences between the genotypes with significant line-by-field interaction for VARI and GRV (Table S4). GLI had some correlation with late-season TSWV at the Gibbs location (R of 0.53) but not significantly with any other traits. At Gibbs, VARI had a correlation of -0.78 with mid-season TSWV, which became increasingly negative to -0.92 with end-season TSWV and -0.83 with leaf spot (Table 3). At Bowen, the correlations were -0.8 for mid-season TSWV and -0.88 for leaf spot. At Gibbs, the correlation of GRV with mid-season TSWV, end-season TSWV, and leaf spot was -0.82, -0.85 and -0.79, respectively. At Bowen, the correlations were -0.75 for mid-season TSWV and -0.83 for leaf spot. The two indices also correlated well with pod weight, especially at Bowen, where the correlation was 0.82 and 0.81 for VARI and GRV, respectively (Table 3).

Table 3. Correlations between red green blue (RGB) indices and manually collected data.

Trait	Spectrum	Formula	Citation	Field	Pod Weight	TSWV (MS)	TSWV (LS)	Leaf Spot (LS)
Visible Atmospherically Resistant Index (VARI)	RGB	(G − R)/(G + R − B)	[54]	Bowen	0.82	−0.8	NA	−0.88
Visible Atmospherically Resistant Index (VARI)	RGB	(G − R)/(G + R − B)	[54]	Gibbs	0.6	−0.78	−0.92	−0.83
Green Vegetation Index-R (GRV)	RGB	(G − R)/(G + R)	[55]	Bowen	0.81	−0.75	NA	−0.83
Green Vegetation Index-R (GRV)	RGB	(G − R)/(G + R)	[55]	Gibbs	0.58	−0.82	−0.85	−0.79
Green Leaf Index (GLI)	RGB	(G × 2 − R − B)/(G × 2 + R + B)	[56]	Bowen	0.01	−0.02	NA	0.16
Green Leaf Index (GLI)	RGB	(G × 2 − R − B)/(G × 2 + R + B)	[56]	Gibbs	−0.18	0.14	0.53	0.40

MS: mid-season; LS: late-season.

Mid-season CTD showed no significant differences between the lines (Table 1). There were significant differences among the lines for end-season CTD with no sample-by-field interaction (Tables 1 and S4). There was a strong correlation between end-season CTD and leaf spot (R = −0.82) and some correlation with end-season TSWV at Gibbs (−0.63). For pod weight, the correlation was 0.82 at Bowen and 0.65 at Gibbs (Table 4).

Table 4. Correlations between multispectral indices and manually collected data.

Trait	Spectrum	Formula	Citation	Leaf Spot	TSWV [a]	Pod Weight Gibbs	Pod Weight Bowen
Chlorophyll Index-RE (CIRE)	Multispectral	IR/(RE − 1)	[57]	−0.95	−0.80	0.43	0.84
Difference Vegetation Index (DVI)	Multispectral	IR − R	[58]	−0.95	−0.85	0.45	0.84
Green Normalized Difference Vegetation Index (GNDVI)	Multispectral	(IR − G)/(IR + G)	[59]	−0.92	−0.94	0.49	0.81
Normalized Green (NG)	Multispectral	G/(IR + R + G)	[60]	0.92	0.94	0.52	0.80
Ratio Vegetation Index (RVI)	Multispectral	IR/R	[61]	−0.93	−0.90	0.55	0.84
Normalized Difference Vegetation Index (NDVI)	Multispectral	(NIR − R)/(NIR + R)	[62]	−0.93	−0.86	0.49	0.81
Optimized Soil Adjusted Vegetation Index (OSAVI)	Multispectral	(1 + 0.16)(IR − R)/(IR + R + 0.16)	[63]	−0.94	−0.85	0.48	0.82
Soil Adjusted Vegetation Index (SAVI)	Multispectral	(1 + 0.5)(IR − R)/(IR + R + 0.5)	[64]	−0.95	−0.85	0.47	0.83
Triangular Vegetation Index (TVI)	Multispectral	0.5 × (120 × (IR − G) − 200 × (R − G))	[65]	−0.95	−0.83	0.45	0.83
End season canopy temperature depression	Thermal	NA	NA	−0.82	−0.63	0.65	0.82

[a] Data for Gibbs late-season.

The multispectral indices were all significantly different, without interaction, and generally showed strong correlations with the disease scores (Tables 4 and S4). For leaf spot, CIRE, DVI, SAVI, and TVI were best correlated with an R of 0.95. In the case of TSWV ratings which were only collected at Gibbs, the best correlations were derived from GNDVI and NG with an R of 0.94. The range of correlations with pod weight were 0.43–0.55 at

Gibbs and 0.8–0.84 at Bowen. Consistent with the strong correlations, the indices ranked the lines comparably with the manual data (Table S5).

Generally, the mean of most traits was comparable to the value of Fleur 11 (Table 1) and varied from the cultivated checks, Florunner and Tifguard, which had better performance than the population. This was expected, since the CSSLs have the genetic background of Fleur 11. For the agronomic traits studied, the broad sense heritabilities were comparable between fields and ranged from 0.4 for mid-season TSWV to 0.74 for pod weight at Bowen. This is indicative of significant and reliable genetic influence on trait variations, a fact also attested by the low standard errors of the trait means. The lowest heritability for significant traits was 0.2 for end-season CTDs, while the rest of the indices, with the exception of GLI at Bowen, had generally high heritabilities. Since the genetic background of the population is known to be uniform, any variation is hypothesized to be a result of introgression effects from wild chromosome segments.

Multicomparison testing was carried out to evaluate how the individual lines differ from Fleur 11 in the different traits (Table S6). It was evident that the three lines, CSSL 84, CSSL 100, and CSSL 111, were the most outstanding in all traits, with the introgressions making them clearly distinct from Fleur 11.

3.3. Belowground Phenotyping

The initial output of a GPR scan is a radargram of the reflected waveform over time, known as a B Scan. The various pipelines for signal processing resulted in the conversion of the B Scans to 13 variables of quantitative data for each pipeline that could be evaluated as proxies for manually collected pod weight data (Table S7). The GPR variables showed significant differences between the genotypes at Bowen. However, the opposite observation was made for Gibbs, as the variables did not show significant differences between the genotypes (Table 5).

Table 5. Summary of GPR variables that showed significant correlations with pod weight.

GPR Variable	Pipeline	Field	Significance of GPR Variable	Mean	Max	Min	SE	Fleur 11	Correlation	Significance of Correlation with Pod Weight
p1_freq_1	1	Bowen	*	0.37	0.459	0.254	0.009	0.35	−0.512	**
p2_freq_1	2	Bowen	*	0.37	0.464	0.259	0.009	0.35	−0.512	**
p3_freq_1	3	Bowen	*	0.34	0.438	0.222	0.010	0.32	−0.518	**
p1_freq_1	3	Gibbs	NS	0.29	0.352	0.246	0.0038	0.35	−0.391	*
p2_freq_1	2	Gibbs	NS	0.29	0.350	0.247	0.0038	0.35	−0.407	*
p3_freq_1	3	Gibbs	NS	0.23	0.266	0.206	0.0026	0.27	−0.453	*
p3_freq_3	3	Gibbs	NS	0.07	0.077	0.063	0.0007	0.07	−0.405	*
p3_freq_4	3	Gibbs	NS	0.06	0.071	0.057	0.0006	0.07	−0.420	*
p3_freq_5	3	Gibbs	NS	0.06	0.068	0.054	0.0006	0.06	−0.409	*
p3_freq_6	3	Gibbs	NS	0.06	0.066	0.053	0.0006	0.06	−0.449	*
p3_freq_7	3	Gibbs	NS	0.06	0.066	0.054	0.0005	0.06	−0.432	*
p3_freq_8	3	Gibbs	NS	0.06	0.065	0.053	0.0005	0.06	−0.440	*
p3_freq_9	3	Gibbs	NS	0.06	0.064	0.052	0.0006	0.06	−0.428	*
p3_freq_10	3	Gibbs	NS	0.06	0.064	0.051	0.0006	0.06	−0.411	*
p3_freq_11	3	Gibbs	NS	0.06	0.064	0.051	0.0006	0.06	−0.430	*
p3_freq_12	3	Gibbs	NS	0.06	0.064	0.052	0.0006	0.06	−0.409	*
p3_freq_13	3	Gibbs	NS	0.06	0.065	0.052	0.0006	0.06	−0.437	*

NS: $p > 0.05$; * $p \leq 0.05$; ** $p \leq 0.01$.

Considerable correlations were observed between the coefficients of GPR variables and those of manual pod weight of the genotypes. At Bowen, three variables had significant

correlations ($p < 0.05$). The variables corresponded to frequency one of pipeline one (p1_freq_1, R = −0.512), pipeline two (p2_freq_1, R = −0.512), and pipeline three (p3_freq_1, R = −0.516) (Figure 4a–c). Similarly, at Gibbs, the variable representing the first frequency for the pipelines had a significant correlation with pod weight ($p < 0.05$) with values of R = −0.391, R = −0.407 and R = −0.453 for p1_freq_1, p2_freq_1, and p3_freq_1, respectively (Figure 4d,e). However, at Gibbs, contrary to the observation at Bowen, all frequency variables derived from pipeline three, with the exception of frequency 2, also had significant correlations with pod weight at $p < 0.05$ and R between −0.449 and −0.405 (Table 5).
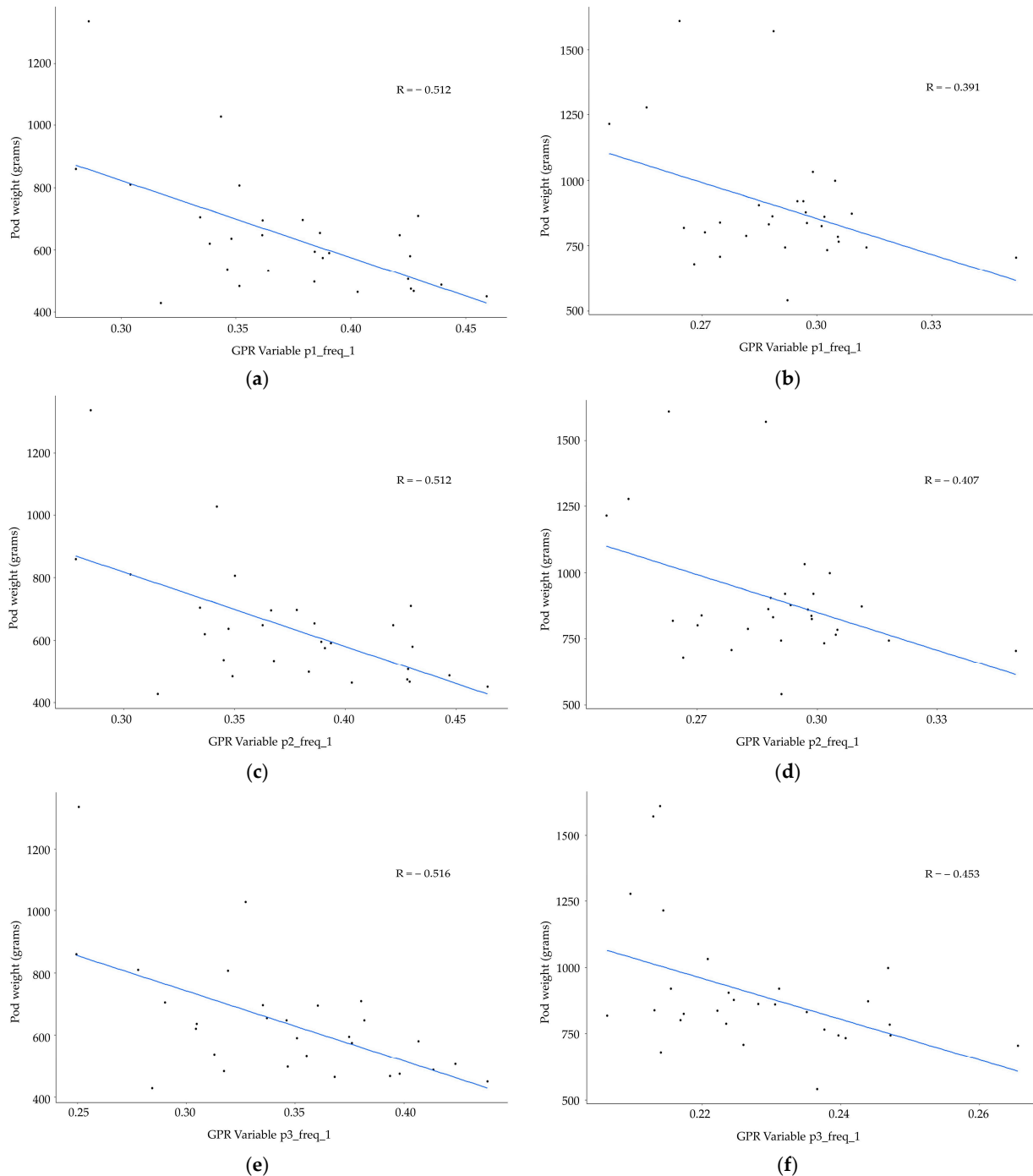
Figure 4. Correlation between pod weight and GPR variables extracted from frequency 1 using pipeline 1 (**a**), pipeline 2 (**b**), pipeline 3 (**c**), at Bowen and pipeline 1 (**d**), pipeline 2 (**e**), pipeline 3 (**f**), at Gibbs.

The ranking capacity of the variables with significant correlations were evaluated by comparing their ability to rank the top and bottom ten genotypes in comparison to manual pod weight (Figure 5 and Table S8). For Bowen, frequency one of all three pipelines captured five of the top genotypes while pipeline one and two captured six of the bottom genotypes and pipeline three captured five of the bottom genotypes. Among the top genotypes detected by all pipelines were the cultivated checks, Florunner (ranked first) and Tifguard (ranked third), as well as CSSL 84 (ranked second). CSSL 111 was ranked seventh by pipelines one and two, and eleventh by pipeline three, while CSSL 100 had an intermediate rank for all pipelines. Curiously, the lowest-performing CSSL 55 was ranked among the top ten at rank four for all pipelines. At Gibbs, frequency one of pipelines one and two captured four of the top genotypes, while pipeline three captured five. For the bottom ranks, frequency one of pipelines one and two captured five, and pipeline three captured seven of the bottom genotypes. The rest of the frequencies of pipeline three that had significant correlations performed marginally worse than frequency one, capturing four of the top genotypes (except frequency seven, which captured five) and three of the bottom genotypes (except frequency four, which captured two). This indicated that, similar to Bowen, the first frequency is sufficient for detecting pod weight. All three pipelines ranked among the top for the cultivated check Tifguard (ranked first by pipelines one and two, and seventh by pipeline 3), CSSL 100 (ranked second by all three pipelines), and CSSL 84 (ranked third by pipeline one and two and five by pipeline 3), while CSSL 111 had an intermediate rank.
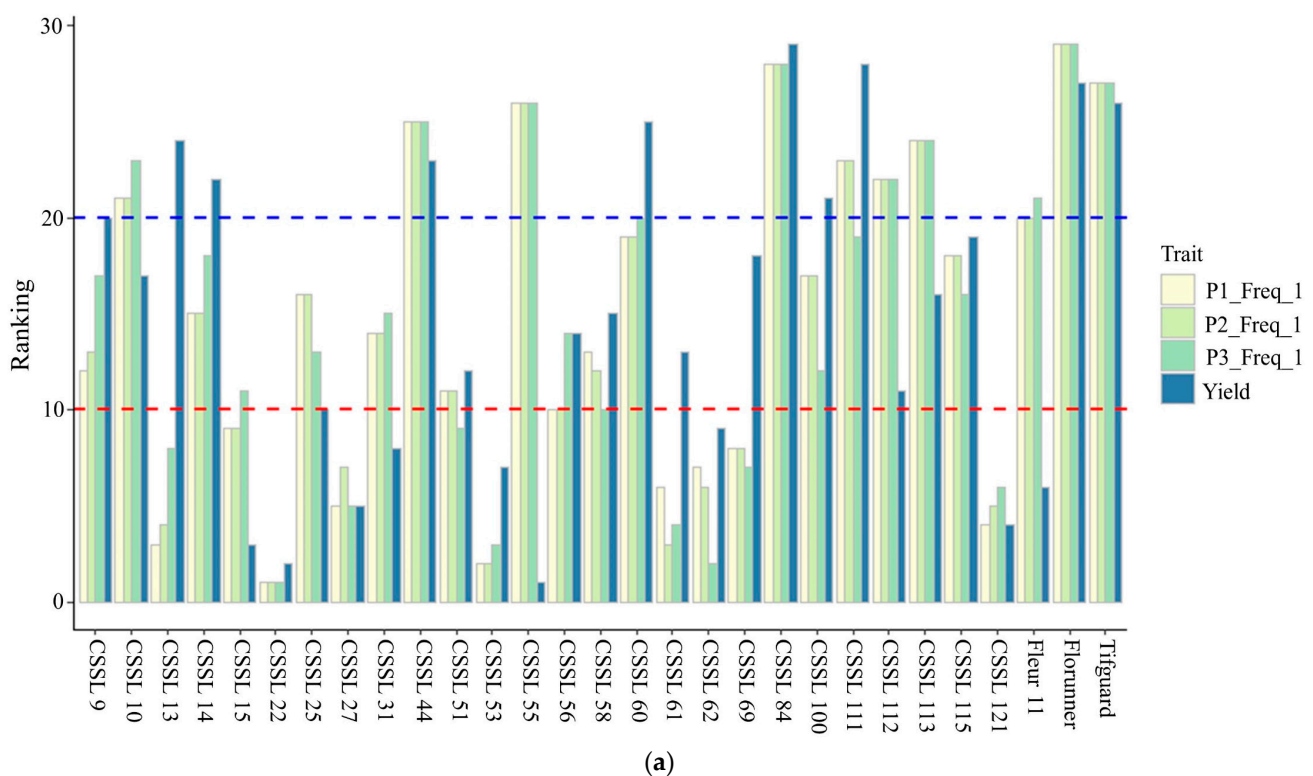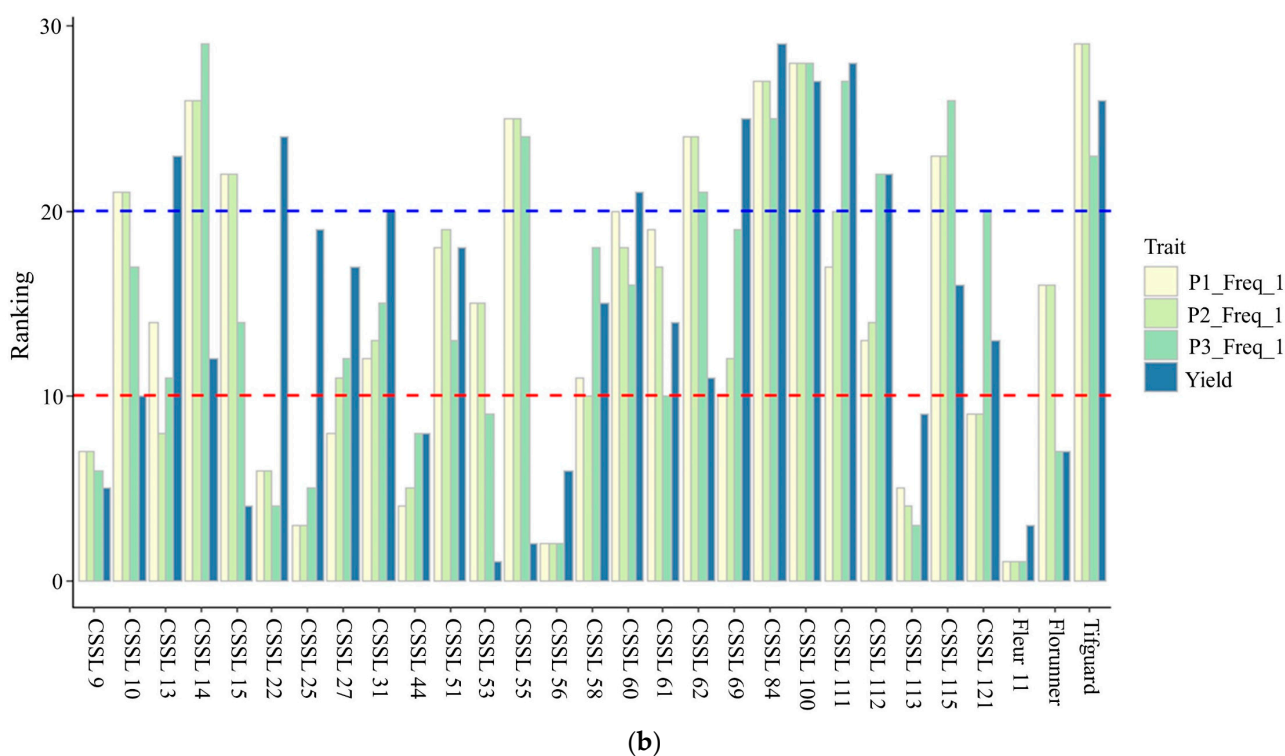

(a)

Figure 5. *Cont.*

(**b**)

Figure 5. Comparison of the ability of the GPR variables to rank the lines relative to pod weight at Bowen (**a**) and Gibbs (**b**). Levels above the blue dashed line highlight lines ranked among the top 10 by pod weight, while levels below the red dashed line highlight lines ranked among the bottom 10 by pod weight.

4. Discussion

Since the cultivated background of the population, Fleur 11, is a Spanish variety predominantly grown in West Africa, there was little expectation that the CSSLs would have agronomic performance similar to those of runner varieties that are highly adaptable in Georgia. The genotypes Tifguard and Florunner were used as adapted runner-type checks. Tifguard is a high-yield cultivar with field resistance to TSWV [66], while Florunner is high-yielding but susceptible to TSWV [67,68]. Both genotypes are susceptible to early and late leaf spot. TSWV causes spotted wilt disease in peanut and was first reported in the US in 1974 [69]. The virus is transmitted by thrips and leads to drastic losses of yield on infected peanut plants [70,71]. In the 1980s and 1990s, severe epidemics that resulted in yield losses of up to USD 40 million were reported in Georgia alone by Bertrand [72], cited in Srinivasan et al. [73]. The use of insecticides to control thrips does not provide sufficient protection against TSWV [74]. This means that the primary strategy for combating the disease is by using cultivars with genetic resistance. Examples of released TSWV-resistant cultivars include Southern Runner [75], Georgia Green [76], Georgia-06G [77], Tifguard [66], and Georgia-09B [78].

Of equally devastating consequences to peanut production are leaf spot diseases. These are classified into early leaf spot, caused by *Passalora arachidicola* (*Hori*) U. Braun (syn. *Cercospora arachidicola*) and late leaf spot, caused by *Nothopassalora personata* (Berk. & M.A. Curtis) U. Braun, C. Nakash., Videira & Crous (syn. *Cercosporidium personatum*) [79]. The two are distinguishable by the color and location of the lesions that they form. ELS typically forms brown lesions on the adaxial (upper) side of the leaves, while LLS forms black lesions on the abaxial (under) side of the leaves [79]. While the diseases can co-occur in the field, the onset of ELS is usually earlier in the season, while for LLS, it is later in the season [80,81]. Management of both diseases is primarily by the costly, regular application of fungicides [82,83]. As with TSWV, sources of genetic resistance for both leaf spots are available, which when used in combination with optimum management

practices lead to reduced costs and losses. Georganic is a cultivar with resistance to leaf spot. Georganic and Tifrunner, both of which were derived from PI 203396, also have resistance to TSWV [84,85]. The most widely utilized source of genetic resistance to leaf spot was from the wild diploid *Arachis cardenasii*, that was introduced into *A. hypogaea* via the hexaploid route to interspecific hybridization [86]. From these introgression lines, GP-NC WS 16, which is resistant to multiple diseases such as ELS, Cylindrocladium black rot (CBR), Sclerotinia blight (SB), and TSWV, was developed [87]. This line has been used as the source of resistance to several populations, including the peanut nested association mapping (NAM) population [88]. Other leaf spot-resistant cultivars derived from the *A. cardenasii* resistance source are the Indian cultivars ICGV 87165 [89] and GPBD 4 [9,90], as well as the Brazilian cultivar IAC Sempre Verde [91].

4.1. Performance of the CSSLs under TSWV and Leaf Spot Pressure

The occurrence of both TSWV and leaf spot diseases provided the opportunity to evaluate the CSSL population for the diseases. CSSL 100, CSSL 84, CSSL 15, and CSSL 111 had superior performance relative to Fleur 11 and the rest of the CSSLs. This indicated that wild chromosome segments conferred some level of disease protection for these lines. Their performance was comparable to that of the resistant check Tifguard. Paradoxically, this good performance was also comparable to that of the notoriously susceptible Florunner. However, qualitative assays of the root tips of the resistant CSSLs and Fleur 11 using immunostrips confirmed that the absence of typical canopy chlorosis was due to the absence of TSWV in the resistant lines [69]. The CSSLs, being Spanish varieties, have a short growing cycle of fewer than 120 days, in contrast to the runner checks that mature at 140 days. With more days of observation, the contrast between the two runner checks and CSSLs may have been more apparent, though the possibility of reduced disease pressure in the year of study cannot be ruled out. However, for these CSSLs, the combination of disease resistance and shorter growing cycle were sufficient to provide adequate protection against TSWV in the Georgia growing environment.

At the time of rating, both early and late leaf spot were observed in the field, with ELS being predominant. As such, the leaf spot rating did not distinguish between the two diseases. The same four lines were superior to Fleur 11 and the rest of the CSSLs, with their performance comparable to Tifguard and Florunner. Under the management practices employed, it was clear that the superior CSSLs had genetic-based suppression of leaf spot. Previously, [*A. ipaensis* X *A. duranensis*]^{4X}, which is the source of introgressions for the CSSLs, was observed to have late leaf spot resistance. BC1F5 lines derived from crossing this allotetraploid to IAC-886, a derivative of the leaf spot susceptible Florunner, were shown to have resistance to LLS [92,93]. Our results suggest that, indeed, wild derived introgressions may have conferred some level of leaf spot resistance to these lines.

4.2. Evaluation of TSWV and Leaf Spot using Vegetative Indices

Strong correlations were observed between disease scores and various image-based vegetative indices. Among the RGB indices, VARI and GRV, which were derived from mid-season ratings, were able to accurately estimate TSWV and leaf spot disease at the end of the season. VARI was designed to remotely estimate the vegetation fraction of canopies with less sensitivity to differences in atmospheric conditions [54]. The index is closely associated with the leaf pigment components, chlorophyll, and carotenoids [94]. It has been used to study green biomass in maize [95], to discriminate between water stress and nitrogen stress in maize [96], and in harvest date optimization in soybean [97]. The GRV index was a modification of VARI and, thus, it had a similar performance with slightly greater sensitivity than VARI. These indices were derived from RGB images taken by a GoPro digital camera. Their informativeness and ability to select the best lines (Table S5) show that, together with the availability of low-cost UAVs, they may be a convenient way to deploy HTP for disease phenotyping by exploiting electromagnetic radiation within the visible range.

Multispectral indices are derived from the canopy reflectance of specific wavelengths in the near-infrared (NIR; 750–1350 nm) as opposed to visible (350–750 nm) regions of the electromagnetic spectrum [98]. Their informativeness is premised on the fact that healthy vegetation absorbs visible light while strongly reflecting NIR. On the contrary, vegetation in poor health absorbs most of the NIR (Mullan, 2012). Spectral indices take advantage of these properties and typically depends on the maximization of differences between the red wavelengths and NIR wavelengths to indicate plant health [98,99]. Examples include the simplest index, known as the ratio vegetative index (RVI) [61], and the most widely used NDVI [62]. While maintaining the same principles, other indices have been developed by modifying parameters to increase their sensitivity to various physiological properties of plants [100]. An example of this is the incorporation of the green channel into NDVI to form GNDVI [59]. Another example is increasing the reflectance of leaf chlorophyll by incorporating red edge (RE) in the index, as in the case of CIRE, which is a modification of the simple index, RVI [61]. Examples of other modifications include adjustments to correct for soil background in indices such as SAVI [64] and its optimized form, OSAVI [63].

Taking these relationships into consideration, it is no surprise that all the multispectral indices we used were comparable with each other and had very strong correlations with the manual disease ratings. Essentially, the indices were detecting the state of the canopy health and not necessarily discriminating between the two diseases nor determining the underlying pathophysiology. The superior CSSLs that were previously not known to have resistance were ranked high by all the indices, showing their sufficiency in phenotyping for this population. All the same, we considered GNDVI to be a representative index for multispectral phenotyping of the population in this study (Figure 6).
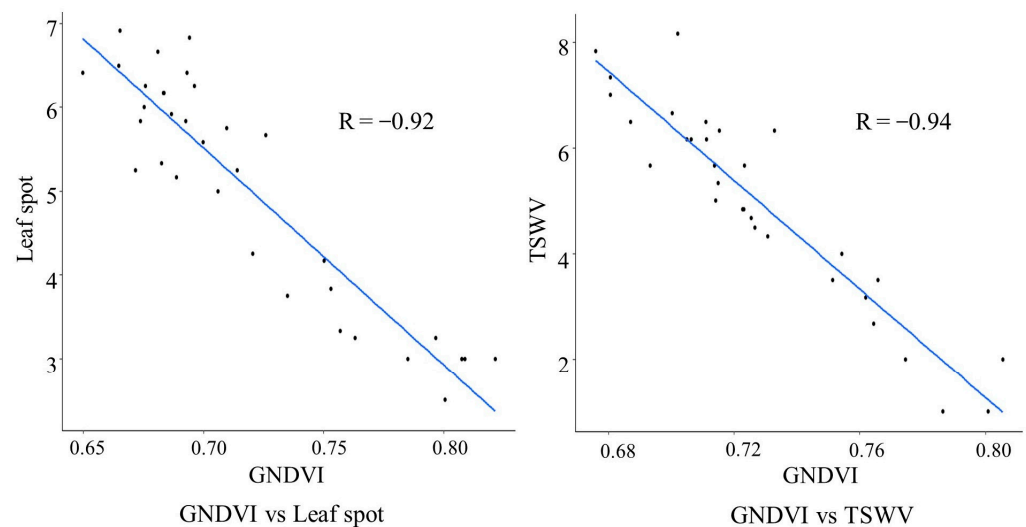

Figure 6. Correlations of green normalized difference vegetative index (GNDVI), one of the multispectral indices used with leaf spot rated at Gibbs and Bowen, and tomato spotted wilt virus TSWV, rated at Gibbs.

The four lines with significantly superior pod weight compared to Fleur 11 showed that introgressions from the wild could be used to improve this important economic trait. In fact, CSSL 69 has been demonstrated to have beneficial introgressions that increase pod and seed size and is a source for pyramiding 100-seed weight QTLs [101]. However, introgressions that conferred protection from the disease were also responsible for the improved performance. This is apparent, especially considering that CSSL 69 had significantly higher pod weight than Fleur 11 at Gibbs, but its disease susceptibility reduced its performance relative to the other three. At Bowen, because of the higher disease pressure, its pod weight performance was reduced to normal. It was impressive that the pod weight of the un-adapted CSSLs with a Spanish background were comparable to those of the high-yielding Tifguard and Florunner. A factor that may have reduced the pod weight of the checks was

the earlier harvest time. Hence the pod-filling process may not have been complete, leading to reduced weight. Even with that taken into account, the performance of the CSSLs is no less impressive. The RGB, multispectral, and CTD indices correlated strongly with pod weight, particularly at Bowen, where the leaf spot pressure was more severe. This points more to a relationship between plant health and pod weight rather than the ability to select for pod weight based on the indices.

4.3. Use of GPR for Pre-Harvest Pod Weight Phenotyping

This is among the first research demonstrating the use of GPR as a peanut phenotyping tool, and the first evaluation of peanut belowground biomass using a frequency-based analysis. Preharvest evaluation of belowground biomass is an area of interest in peanut research. While canopy traits are important due to the pervasiveness of a plethora of foliar diseases, the geocarpic nature of peanut makes belowground phenotyping an area of particular importance. So far, any subsurface evaluation of traits such as white mold, root system architecture, and most importantly, yield and its components, has necessitated destructive digging of the plants at the end of the season. This study implemented a potentially revolutionary technique in studying peanut pod traits prior to harvest.

GPR technology has been used extensively as a noninvasive way to detect a coarse large structure belowground biomass, primarily tree roots, with considerable success [102–104]. However, its application for fine biomass structure detection, which would be ideal for agricultural research, has been limited by the fact that such structures are typically below the detection threshold of commonly used GPR frequencies, which are typically in the 500–1500 MHz range [105–107]. Still, the technology has been applied in root phenotyping of crops such as winter wheat and energy cane, though rather than describing root architecture, root cohort parameters such as biomass and density were studied [46,107]. An important case where it was used was the study of the root bulking rate of cassava, a crop whose economic potential is stored belowground. In this case, GPR detection was sufficient, with a correlation of up to 0.65 [48] and 0.79 with the ability to discriminate between varieties [40].

Like cassava, the economic yield component of peanut is situated belowground, since after flowering, the peanut develops a peg that grows downwards, penetrates the soil, and elongates sideways to form the pods. Pod formation occurs in the pod zone, a region that is approximately 4 cm below the surface and hence shallower than the root zone. This made the choice of a GPR system with a high central frequency antenna (1800 MHz) appropriate for this study, since higher frequencies promise higher radar resolution at shallow depths [107]. The resultant radargrams were processed using three different pipelines to derive quantitative data from the reflectance of GPR frequencies ranging from 1–13 GHz for association with pod weight. The features were grouped into 13 variables, each representing a frequency band, such that variable 1 represented frequencies within 1 GHz and so on.

These variables yielded useful information that could be related to the belowground biomass properties of the population, suggesting that GPR had potential utility for the non-destructive preharvest HTP of peanut. Statistical analysis of the variables showed disparity in the performance of GPR between the Gibbs and Bowen fields. This may be attributed to the more intense disease pressure at Bowen, particularly leaf spot. This may have resulted in severe penalties, as observed by the more intense inverse correlation between pod weight and late-season leaf spot at Bowen than at Gibbs (R = −0.79 and R = −0.47, respectively). Hence, the variation in GPR-detectable biomass may have been more pronounced at Bowen than at Gibbs. It is also worth considering that the soil condition differences between the two fields may have contributed to the difference in results. While standardization of the GPR processing pipeline would be ideal for the automation and applicability of the technology across different geographic sites, with respect to the current implementation, optimization of the processing pipelines for each specific site may be required.

For all three analysis pipelines used to derive quantitative GPR features, variable one, corresponding to the seven frequency bands within 1 GHz was the most informative. This was within expectation since the central frequency of the GPR system used was 1.8 GHz. The comparable performance of the three pipelines indicated that either was sufficient for GPR processing with only a slight bias for pipeline three. Combining the features by calculating the area under the frequency curve for the DFTs was also an effective way to derive variables from GPR output that could be implemented into a breeder's analysis protocol similar to other conventional data. Linear regression of these variables yielded coefficients that correlated relatively well with the coefficients of manual pod weight data. Specifically, there was a negative correlation between the GPR features based on Fourier transform and pod weight. The amplitude of the Fourier coefficients is typically related to greater or smaller GPR signal variability at the specified frequency. With this assumption, the negative correlations reported in this study imply that smaller GPR signal variability is associated with greater peanut pod weight for these frequencies. A plot with more pods belowground may mean a greater clustering of peanut pods with less soil in between the peanut pods and thus the smaller GPR signal variability, as opposed to a plot with fewer pods where more soil is present between the peanut pods resulting in greater signal variability. Since this is the first application of a frequency-based GPR analysis to peanut pod weight assessment, our interpretations are only based on the results of this study. Image thresholding analysis demonstrated a negative correlation to GPR features based on the mean of the signal amplitude and positive correlations based on the standard deviation of the signal amplitude [47].

The R values of up to -0.51 compare well with the R = 0.65 and 0.79 observed in cassava [40,48], considering the much smaller belowground biomass characteristic of peanut. Despite the moderate correlations, the variables gave reasonable ranking by pod weight for the population when compared with the manual data, with the top CSSLs and check varieties consistently featuring at the top. A sticking anomaly was the observation of CSSL 55, which has a lower pod weight among the top genotypes based on GPR ranks, which contributed to lowering the correlations. This may be attributed to the fact that GPR detects reflections of electromagnetic frequencies that are converted to an image from which the volumetric mass is estimated as pod weight. On the other hand, the manual pod weight measures only mass. Generally, genotypes with bigger pod sizes tend to have more pod weight mass; however, this is not always the case since other factors, such as the number of pods per plant, pod filling, and maturity at harvest, also affect the final pod weight. An example is CSSL 100, which generally has smaller pods but is among the best-performing genotypes by weight. With more research towards the improvement of GPR methods and analysis for fine biomass detection, it is conceivable that belowground HTP will be adopted with higher frequency in peanut research.

5. Conclusions

The findings of this study highlight novel phenomic approaches by which the peanut breeding pipeline can maintain and improve its current state. Examination of the CSSL population shows that alleles from peanut wild relatives can confer agronomically beneficial traits to the cultivated. The use of both aerial and belowground phenomic techniques has the potential to radically transform the peanut breeding pipeline by increasing the speed and precision of phenotype data acquisition. These techniques will facilitate the identification and speedy release of novel and better-adapted peanut varieties, hence improving the process of peanut breeding.

Supplementary Materials: The following supporting information can be downloaded at: https://www.mdpi.com/article/10.3390/agronomy13051223/s1. Table S1: GPR DFT raw data based on pipeline 1 for all plots; Table S2: GPR DFT raw data based on pipeline 2 for all plots; Table S3: GPR DFT raw data based on pipeline 3 for all plots; Table S4: Summary analysis of interactions between samples and field for manually collected data and spectral indices; Table S5: Ranking of the chromosome segment substitution lines (CSSLs) based on Green Normalized Difference Vegetation

Index (GNDVI), Visible Atmospherically Resistant Index (VARI), and Green Vegetation Index-R (GRV). The indices generally rank the lines similarly to the manual data, showing their capacity for selection in this population; Table S6: The effects of introgressions on the traits that were manually collected. Lines with significant introgression effects are presented. For TSWV late season, CSSL 10, CSSL 84, and CSSL 111, which are not statistically significant, are highlighted because of their high numeric effects. The introgression effects were calculated as percentages relative to the cultivated Fleur 11; Table S7: Summary statistics of all GPR variables; Table S8: Comparison of CSSL ranking ability between manual pod weight data and GPR variables that showed significant correlations with pod weight at Bowen and Gibbs. The CSSLs are ranked based on pod weight performance. The ranking by the GPR variables is indicated in the respective columns for each variable. Green font indicates the top 10 CSSLs as ranked by pod weight, while purple font indicates the bottom 10 CSSLs as ranked by pod weight.

References

1. Fonceka, D.; Tossim, H.-A.; Rivallan, R.; Vignes, H.; Lacut, E.; de Bellis, F.; Faye, I.; Ndoye, O.; Leal-Bertioli, S.C.M.; Valls, J.F.M.; et al. Construction of chromosome segment substitution lines in peanut (*Arachis hypogaea* L.) using a wild synthetic and QTL mapping for plant morphology. *PLoS ONE* **2012**, *7*, e48642. [CrossRef] [PubMed]
2. Seijo, J.G.; Lavia, G.I.; Fernández, A.; Krapovickas, A.; Ducasse, D.; Moscone, E.A. Physical mapping of the 5S and 18S-25S rRNA genes by FISH as evidence that *Arachis duranensis* and *A. ipaensis* are the wild diploid progenitors of *A. hypogaea* (Leguminosae). *Am. J. Bot.* **2004**, *91*, 1294–1303. [CrossRef] [PubMed]
3. Moretzsohn, M.C.; Gouvea, E.G.; Inglis, P.W.; Leal-Bertioli, S.C.M.; Valls, J.F.M.; Bertioli, D.J. A study of the relationships of cultivated peanut (*Arachis hypogaea*) and its most closely related wild species using intron sequences and microsatellite markers. *Ann. Bot.* **2013**, *111*, 113–126. [CrossRef]
4. Kochert, G.; Stalker, T.; Gimenes, M.; Galgaro, L.; Lopes, C.R.; Moore, K. RFLP and cytogenetic evidence on the origin and evolution of allotetraploid domesticated peanut, *Arachis hypogaea* (Leguminosae). *Am. J. Bot.* **1996**, *83*, 1282–1291. [CrossRef]
5. Foncéka, D.; Hodo-Abalo, T.; Rivallan, R.; Faye, I.; Sall, M.; Ndoye, O.; Fávero, A.P.; Bertioli, D.J.; Glaszmann, J.-C.; Courtois, B.; et al. Genetic mapping of wild introgressions into cultivated peanut: A way toward enlarging the genetic basis of a recent allotetraploid. *BMC Plant Biol.* **2009**, *9*, 103. [CrossRef]
6. Hopkins, M.S.; Casa, A.M.; Wang, T.; Mitchell, S.E.; Dean, R.E.; Kochert, G.D.; Kresovich, S. Discovery and Characterization of Polymorphic Simple Sequence Repeats (SSRs) in Peanut. *Crop Sci.* **1999**, *39*, 1243. [CrossRef]
7. Varshney, R.K.; Mahendar, T.; Aruna, R.; Nigam, S.N.; Neelima, K.; Vadez, V.; Hoisington, D.A. High level of natural variation in a groundnut (*Arachis hypogaea* L.) germplasm collection assayed by selected informative SSR markers. *Plant Breed.* **2009**, *128*, 486–494. [CrossRef]
8. Stalker, H.T.; Tallury, S.P.; Ozias-Akins, P.; Bertioli, D.; Bertioli, S.C.L. The value of diploid peanut relatives for breeding and genomics. *Peanut Sci.* **2013**, *40*, 70–88. [CrossRef]
9. Stalker, H.T. Utilizing wild species for peanut improvement. *Crop Sci.* **2017**, *57*, 1102–1120. [CrossRef]
10. Fávero, A.P.; Simpson, C.E.; Valls, J.F.M.; Vello, N.A. Study of the evolution of cultivated peanut through crossability studies among *Arachis ipaensis*, *A. duranensis*, and *A. hypogaea*. *Crop Sci.* **2006**, *46*, 1546–1552. [CrossRef]
11. Bertioli, D.J.; Jenkins, J.; Clevenger, J.; Dudchenko, O.; Gao, D.; Seijo, G.; Leal-Bertioli, S.C.M.; Ren, L.; Farmer, A.D.; Pandey, M.K.; et al. The genome sequence of segmental allotetraploid peanut *Arachis hypogaea*. *Nat. Genet.* **2019**, *51*, 877–884. [CrossRef] [PubMed]
12. Bertioli, D.J.; Cannon, S.B.; Froenicke, L.; Huang, G.; Farmer, A.D.; Cannon, E.K.S.; Liu, X.; Gao, D.; Clevenger, J.; Dash, S.; et al. The genome sequences of *Arachis duranensis* and *Arachis ipaensis*, the diploid ancestors of cultivated peanut. *Nat. Genet.* **2016**, *48*, 438–446. [CrossRef]

13. Clevenger, J.; Chu, Y.; Chavarro, C.; Agarwal, G.; Bertioli, D.J.; Leal-Bertioli, S.C.M.; Pandey, M.K.; Vaughn, J.; Abernathy, B.; Barkley, N.A.; et al. Genome-wide SNP genotyping resolves signatures of selection and tetrasomic recombination in Peanut. *Mol. Plant* **2017**, *10*, 309–322. [CrossRef] [PubMed]

14. Pandey, M.K.; Agarwal, G.; Kale, S.M.; Clevenger, J.; Nayak, S.N.; Sriswathi, M.; Chitikineni, A.; Chavarro, C.; Chen, X.; Upadhyaya, H.D.; et al. Development and evaluation of a high density genotyping "Axiom-Arachis" Array with 58 K SNPs for accelerating genetics and breeding in groundnut. *Sci. Rep.* **2017**, *7*, 40577. [CrossRef] [PubMed]

15. Clevenger, J.P.; Korani, W.; Ozias-Akins, P.; Jackson, S. Haplotype-based genotyping in polyploids. *Front. Plant Sci.* **2018**, *9*, 564. [CrossRef]

16. Korani, W.; Clevenger, J.P.; Chu, Y.; Ozias-Akins, P. Machine learning as an effective method for identifying true single nucleotide polymorphisms in polyploid plants. *Plant Genome* **2019**, *12*, 180023. [CrossRef]

17. Clevenger, J.; Chu, Y.; Scheffler, B.; Ozias-Akins, P. A developmental transcriptome map for allotetraploid *Arachis hypogaea*. *Front. Plant Sci.* **2016**, *7*, 1–18. [CrossRef]

18. Ozias-akins, P.; Cannon, E.K.S.; Cannon, S.B. Genomic Resources for Peanut Improvement. In *The Peanut Genome; Compendium of Plant Genomes Book Series*; Varshney, R., Pandey, M., Puppala, N., Eds.; Springer: Berlin/Heidelberg, Germany, 2017; pp. 69–91. [CrossRef]

19. Ozias-Akins, P. The orphan legume genome whose time has come: Symposium highlights from the american peanut research education society annual meeting. *Peanut Sci.* **2013**, *40*, 66–69. [CrossRef]

20. Svensgaard, J.; Roitsch, T.; Christensen, S. Development of a mobile multispectral imaging platform for precise field phenotyping. *Agronomy* **2014**, *4*, 322–336. [CrossRef]

21. De Witt, C. *On Competition*; 66.8.; Versl.; Landbouwk Underz: Wagenigen, The Netherlands, 1960.

22. Furbank, R.T.; Tester, M. Phenomics—Technologies to relieve the phenotyping bottleneck. *Trends Plant Sci.* **2011**, *16*, 635–644. [CrossRef]

23. Chen, D.; Neumann, K.; Friedel, S.; Kilian, B.; Chen, M.; Altmann, T.; Klukas, C. Dissecting the phenotypic components of crop plant growthand drought responses based on high-throughput image analysis w open. *Plant Cell* **2014**, *26*, 4636–4655. [CrossRef] [PubMed]

24. Fiorani, F.; Schurr, U. Future scenarios for plant phenotyping. *Annu. Rev. Plant Biol.* **2013**, *64*, 267–291. [CrossRef] [PubMed]

25. Ge, Y.; Bai, G.; Stoerger, V.; Schnable, J.C. Temporal dynamics of maize plant growth, water use, and leaf water content using automated high throughput RGB and hyperspectral imaging. *Comput. Electron. Agric.* **2016**, *127*, 625–632. [CrossRef]

26. Olson, D.; Anderson, J. Review on unmanned aerial vehicles, remote sensors, imagery processing, and their applications in agriculture. *Agron. J.* **2021**, *113*, 971–992. [CrossRef]

27. Cheng, Q.; Xu, H.; Fei, S.; Li, Z.; Chen, Z. Estimation of maize LAI using ensemble learning and UAV multispectral imagery under different water and fertilizer treatments. *Agriculture* **2022**, *12*, 1267. [CrossRef]

28. Rodene, E.; Xu, G.; Delen, S.P.; Zhao, X.; Smith, C.; Ge, Y.; Schnable, J.; Yang, J. A UAV-based high-throughput phenotyping approach to assess time-series nitrogen responses and identify trait-associated genetic components in maize. *Plant Phenome J.* **2022**, *5*, e20030. [CrossRef]

29. Jiang, R.; Sanchez-Azofeifa, A.; Laakso, K.; Wang, P.; Xu, Y.; Zhou, Z.; Luo, X.; Lan, Y.; Zhao, G.; Chen, X. UAV-based partially sampling system for rapid NDVI mapping in the evaluation of rice nitrogen use efficiency. *J. Clean. Prod.* **2021**, *289*, 125705. [CrossRef]

30. Jin, H.; Köppl, C.J.; Fischer, B.M.C.; Rojas-Conejo, J.; Johnson, M.S.; Morillas, L.; Lyon, S.W.; Durán-Quesada, A.M.; Suárez-Serrano, A.; Manzoni, S.; et al. Drone-based hyperspectral and thermal imagery for quantifying upland rice productivity and water use efficiency after biochar application. *Remote Sens.* **2021**, *13*, 1866. [CrossRef]

31. Alabi, T.R.; Abebe, A.T.; Chigeza, G.; Fowobaje, K.R. Estimation of soybean grain yield from multispectral high-resolution UAV data with machine learning models in West Africa. *Remote Sens. Appl. Soc. Environ.* **2022**, *27*, 100782. [CrossRef]

32. Marston, Z.P.D.; Cira, T.M.; Hodgson, E.W.; Knight, J.F.; MacRae, I.V.; Koch, R.L.; Rondon, S. Detection of stress induced by soybean aphid (Hemiptera: Aphididae) using multispectral imagery from unmanned aerial vehicles. *J. Econ. Entomol.* **2020**, *113*, 779–786. [CrossRef]

33. Balota, M.; Oakes, J. Exploratory use of a UAV platform for variety selection in peanut. In *Autonomous Air and Ground Sensing Systems for Agricultural Optimization and Phenotyping*; Society of Photo-Optical Instrumentation Engineers (SPIE) Conference Series; International Society for Optics and Photonics: Washington, DC, USA, 2016; Volume 9866, p. 98660F. [CrossRef]

34. Balota, M.; Oakes, J. UAV remote sensing for phenotyping drought tolerance in peanuts. In *Autonomous Air and Ground Sensing Systems for Agricultural Optimization and Phenotyping II*; Society of Photo-Optical Instrumentation Engineers (SPIE) Conference Series; International Society for Optics and Photonics: Washington, DC, USA, 2017; Volume 10218, p. 102180C. [CrossRef]

35. Abd-El Monsef, H.; Smith, S.E.; Rowland, D.L.; Abd El Rasol, N. Using multispectral imagery to extract a pure spectral canopy signature for predicting peanut maturity. *Comput. Electron. Agric.* **2019**, *162*, 561–572. [CrossRef]

36. Patrick, A.; Pelham, S.; Culbreath, A.; Corely Holbrook, C.; De Godoy, I.J.; Li, C. High throughput phenotyping of tomato spot wilt disease in peanuts using unmanned aerial systems and multispectral imaging. *IEEE Instrum. Meas. Mag.* **2017**, *20*, 4–12. [CrossRef]

37. Sarkar, S.; Ramsey, A.F.; Cazenave, A.B.; Balota, M. Peanut leaf wilting estimation from RGB color indices and logistic models. *Front. Plant Sci.* **2021**, *12*, 713. [CrossRef]

38. Sarkar, S.; Oakes, J.; Cazenave, A.B.; Burow, M.D.; Bennett, R.S.; Chamberlin, K.D.; Wang, N.; White, M.; Payton, P.; Mahan, J.; et al. Evaluation of the U.S. peanut germplasm mini-core collection in the Virginia-Carolina region using traditional and new high-throughput methods. *Agronomy* **2022**, *12*, 1945. [CrossRef]

39. Bagherian, K.; Puhl, R.B.; Bao, Y.; Zhang, Q.; Sanz-Saez, A.; Chen, C.; Dang, P. Phenotyping agronomic traits of peanuts using UAV-based hyperspectral imaging and deep learning. In Proceedings of the ASABE 2022 Annual International Meeting, Houston, TX, USA, 17–20 July 2022. [CrossRef]

40. Delgado, A.; Hays, D.B.; Bruton, R.K.; Ceballos, H.; Novo, A.; Boi, E.; Selvaraj, M.G. Ground penetrating radar: A case study for estimating root bulking rate in cassava (*Manihot esculenta* Crantz). *Plant Methods* **2017**, *13*, 65. [CrossRef]

41. Butnor, J.R.; Doolittle, J.A.; Kress, L.; Cohen, S.; Johnsen, K.H. Use of ground-penetrating radar to study tree roots in the southeastern United States. *Tree Physiol.* **2001**, *21*, 1269–1278. [CrossRef]

42. Butnor, J.R.; Doolittle, J.A.; Johnsen, K.H.; Samuelson, L.; Stokes, T.; Kress, L. Utility of ground-penetrating radar as a root biomass survey tool in forest systems. *Soil Sci. Soc. Am. J.* **2003**, *67*, 1607. [CrossRef]

43. Borden, K.A.; Isaac, M.E.; Thevathasan, N.V.; Gordon, A.M.; Thomas, S.C. Estimating coarse root biomass with ground penetrating radar in a tree-based intercropping system. *Agrofor. Syst.* **2014**, *88*, 657–669. [CrossRef]

44. Borden, K.A.; Thomas, S.C.; Isaac, M.E. Interspecific variation of tree root architecture in a temperate agroforestry system characterized using ground-penetrating radar. *Plant Soil* **2017**, *410*, 323–334. [CrossRef]

45. Borden, K.A.; Anglaaere, L.C.N.; Adu-Bredu, S.; Isaac, M.E. Root biomass variation of cocoa and implications for carbon stocks in agroforestry systems. *Agrofor. Syst.* **2019**, *93*, 369–381. [CrossRef]

46. Liu, X.; Dong, X.; Xue, Q.; Leskovar, D.I.; Jifon, J.; Butnor, J.R.; Marek, T. Ground penetrating radar (GPR) detects fine roots of agricultural crops in the field. *Plant Soil* **2018**, *423*, 517–531. [CrossRef]

47. Dobreva, I.D.; Ruiz-Guzman, H.A.; Barrios-Perez, I.; Adams, T.; Teare, B.L.; Payton, P.; Everett, M.E.; Burow, M.D.; Hays, D.B. Thresholding analysis and feature extraction from 3D ground penetrating radar data for noninvasive assessment of peanut yield. *Remote Sens.* **2021**, *13*, 1896. [CrossRef]

48. Agbona, A.; Teare, B.; Ruiz-Guzman, H.; Dobreva, I.D.; Everett, M.E.; Adams, T.; Montesinos-Lopez, O.A.; Kulakow, P.A.; Hays, D.B. Prediction of root biomass in cassava based on ground penetrating radar phenomics. *Remote Sens.* **2021**, *13*, 4908. [CrossRef]

49. Simpson, C.E. Pathways for introgression of pest resistance into *Arachis hypogaea* L. *Peanut Sci.* **1991**, *18*, 22–26. [CrossRef]

50. ESRI. *ArcGIS Desktop*; Environmental Systems Research Institute: Redlands, CA, USA, 2011.

51. R Core Team. *R: A Language and Environment for Statistical Computing*; R Foundation for Statistical Computing: Vienna, Austria, 2021.

52. Kuznetsova, A.; Brockhoff, P.B.; Christensen, R.H.B. LmerTest package: Tests in linear mixed effects models. *J. Stat. Softw.* **2017**, *82*, 1–26. [CrossRef]

53. Dunnett, C.W. A multiple comparison procedure for comparing several treatments with a control. *J. Am. Stat. Assoc.* **1955**, *50*, 1096–1121. [CrossRef]

54. Gitelson, A.A.; Kaufman, Y.J.; Stark, R.; Rundquist, D. Novel algorithms for remote estimation of vegetation fraction. *Remote Sens. Environ.* **2002**, *80*, 76–87. [CrossRef]

55. Tucker, C.J. Red and photographic infrared linear combinations for monitoring vegetation. *Remote Sens. Environ.* **1979**, *8*, 127–150. [CrossRef]

56. Louhaichi, M.; Borman, M.M.; Johnson, D.E. Spatially located platform and aerial photography for documentation of grazing impacts on wheat. *Geocarto Int.* **2001**, *16*, 65–70. [CrossRef]

57. Gitelson, A.A.; Viña, A.; Ciganda, V.; Rundquist, D.C.; Arkebauer, T.J. Remote estimation of canopy chlorophyll content in crops. *Geophys. Res. Lett.* **2005**, *32*. [CrossRef]

58. Richardson, A.J.; Wiegand, C.L. Distinguishing vegetation from soil background information. *Photogramm. Eng. Rem. S* **1977**, *43*, 1541–1552.

59. Gitelson, A.A.; Kaufman, Y.J.; Merzlyak, M.N. Use of a green channel in remote sensing of global vegetation from EOS-MODIS. *Remote Sens. Environ.* **1996**, *58*, 289–298. [CrossRef]

60. Sripada, R.P.; Heiniger, R.W.; White, J.G.; Weisz, R. Aerial color infrared photography for determining late-season nitrogen requirements in corn. *Agron. J.* **2005**, *97*, 1443–1451. [CrossRef]

61. Jordan, C.F. Derivation of leaf-area index from quality of light on the forest floor. *Ecology* **1969**, *50*, 663–666. [CrossRef]

62. Rouse, J.W., Jr.; Haas, R.H.; Schell, J.A.; Deering, D.W. Monitoring vegetation systems in the great plains with erts. *NASA Spec Publ.* **1974**, *351*, 309–317.

63. Baret, F.; Jacquemoud, S.; Hanocq, J.F. The soil line concept in remote sensing. *Remote Sens. Rev.* **1993**, *7*, 65–82. [CrossRef]

64. Huete, A.R. A soil-adjusted vegetation index (SAVI). *Remote Sens. Environ.* **1988**, *25*, 295–309. [CrossRef]

65. Broge, N.H.; Leblanc, E. Comparing prediction power and stability of broadband and hyperspectral vegetation indices for estimation of green leaf area index and canopy chlorophyll density. *Remote Sens. Environ.* **2001**, *76*, 156–172. [CrossRef]

66. Holbrook, C.C.; Timper, P.; Culbreath, A.K.; Kvien, C.K. Registration of 'Tifguard' Peanut. *J. Plant Regist.* **2008**, *2*, 92. [CrossRef]

67. Anderson, W.F.; Holbrook, C.C.; Culbreath, A.K. Screening the peanut core collection for resistance to tomato spotted wilt virus. *Peanut Sci.* **1996**, *23*, 57–61. [CrossRef]

68. Knauft, D.A.; Gorbet, D.W. Genetic diversity among peanut cultivars. *Crop Sci.* **1989**, *29*, 1417. [CrossRef]

69. Culbreath, A.K.; Todd, J.W.; Brown, S.L. Epidemiology and management of tomato spotted wilt in peanut. *Annu. Rev. Phytopathol.* **2003**, *41*, 53–75. [CrossRef] [PubMed]

70. Culbreath, A.K.; Todd, J.W.; Demski, J.W. Productivity of florunner peanut infected with tomato spotted wilt virus. *Peanut Sci.* **1992**, *19*, 11–14. [CrossRef]

71. Culbreath, A.K.; Todd, J.W.; Gorbet, D.W.; Brown, S.L.; Baldwin, J.; Pappu, H.R.; Shokes, F.M. Reaction of peanut cultivars to spotted wilt. *Peanut Sci.* **2000**, *27*, 35–39. [CrossRef]

72. Bertrand, P.F. 1997 Georgia plant disease loss estimates. *Univ. Ga. Coop. Ext. Pub. Pathol.* **1998**, *81*, 98–107.

73. Srinivasan, R.; Abney, M.R.; Culbreath, A.K.; Kemerait, R.C.; Tubbs, R.S.; Monfort, W.S.; Pappu, H.R. Three decades of managing Tomato spotted wilt virus in peanut in southeastern United States. *Virus Res.* **2017**, *106*, 203–212. [CrossRef] [PubMed]

74. Todd, J.W.; Culbreath, A.K.; Brown, S.L. Dynamics of vector populations and progress of spotted wilt disease relative to insecticide use in peanuts. *Acta Hortic.* **1996**, *431*, 483–490. [CrossRef]

75. Gorbet, D.W.; Norden, A.J.; Shokes, F.M.; Knauft, D.A. Registration of 'Southern Runner' peanut. *Crop Sci.* **1987**, *27*, 817. [CrossRef]

76. Branch, W.D. Registration of 'Georgia Green' peanut. *Crop Sci.* **1996**, *36*, 806. [CrossRef]

77. Branch, W.D. Registration of 'Georgia-06G' peanut. *J. Plant Regist.* **2007**, *1*, 120. [CrossRef]

78. Branch, W.D. Registration of "Georgia-09B" peanut. *J. Plant Regist.* **2010**, *4*, 175–178. [CrossRef]

79. Smith, H.D.; Littrell, H.R. Management of peanut foliar diseases with fungicides. *Am. Phytopathol. Soc.* **1980**, *64*, 356–361.

80. Chu, Y.; Holbrook, C.C.; Isleib, T.G.; Burow, M.; Culbreath, A.K.; Tillman, B.; Chen, J.; Clevenger, J.; Ozias-Akins, P. Phenotyping and genotyping parents of sixteen recombinant inbred peanut populations. *Peanut Sci.* **2018**, *45*, 1–11. [CrossRef]

81. Chu, Y.; Chee, P.; Culbreath, A.; Isleib, T.G.; Holbrook, C.C.; Ozias-Akins, P. Major QTLs for resistance to early and late leaf spot diseases are identified on chromosomes 3 and 5 in peanut (*Arachis hypogaea*). *Front. Plant Sci.* **2019**, *10*, 883. [CrossRef] [PubMed]

82. Woodward, J.E.; Brenneman, T.B.; Kemerait, R.C.; Smith, N.B.; Culbreath, A.K.; Stevenson, K.L. Use of resistant cultivars and reduced fungicide programs to manage peanut diseases in irrigated and nonirrigated fields. *Plant Dis.* **2008**, *92*, 896–902. [CrossRef]

83. Woodward, J.E.; Brenneman, T.B.; Kemerait, R.C.; Culbreath, A.K.; Smith, N.B. Management of peanut diseases with reduced input fungicide programs in fields with varying levels of disease risk. *Crop Prot.* **2010**, *29*, 222–229. [CrossRef]

84. Holbrook, C.C.; Culbreath, A.K. Registration of "Tifrunner" peanut. *J. Plant Regist.* **2007**, *1*, 124. [CrossRef]

85. Holbrook, C.C.; Culbreath, A.K. Registration of "Georganic" Peanut. *J. Plant Regist.* **2008**, *2*, 10–3198. [CrossRef]

86. Company, M.; Stalker, H.T.; Wynne, J.C. Cytology and leafspot resistance in *Arachis hypogaea* x wild species hybrids. *Euphytica* **1982**, *31*, 885–893. [CrossRef]

87. Tallury, S.P.; Isleib, T.G.; Copeland, S.C.; Rosas-Anderson, P.; Balota, M.; Singh, D.; Stalker, H.T. Registration of two multiple disease-resistant peanut germplasm lines derived from *Arachis cardenasii* Krapov. & W.C. Gregory, GKP 10017. *J. Plant Regist.* **2014**, *8*, 86–89. [CrossRef]

88. Holbrook, C.C.; Isleib, T.G.; Ozias-Akins, P.; Chu, Y.; Knapp, S.J.; Tillman, B.; Guo, B.; Gill, R.; Burow, M.D. Development and phenotyping of recombinant inbred line (RIL) populations for peanut (*Arachis hypogaea*). *Peanut Sci.* **2013**, *40*, 89–94. [CrossRef]

89. Moss, J.P.; Singh, A.K.; Reddy, L.J.; Nigam, S.N.; Subrahmanyam, P.; McDonald, D.; Reddy, A.G.S. Registration of ICGV 87165 peanut germplasm line with multiple resistance. *Crop Sci.* **1997**, *37*, 1028. [CrossRef]

90. Gowda, M.; Motagi, B.; Naidu, G.; Diddimani, S.; Sheshagiri, R. GPBD 4: A spanish bunch groundnut genotype resistant to rust and late leaf spot. *Int. Arachis Newsl.* **2002**, *22*, 29–32.

91. Godoy, I.J.; Santos, J.F.; De Carvalho Moretzsohn, M.; Rocha, A.; Moraes, A.; Michelotto, M.D.; Bolonhezi, D.; Nakayama, F.; Soares De Freitas, R.; Bertioli, D.J.; et al. 'IAC SEMPRE VERDE': A wild-derived peanut cultivar highly resistant to foliar diseases. *Crop Breed. Appl. Biotechnol.* **2022**, *22*, e41252232. [CrossRef]

92. Leal-Bertioli, S.C.M.; Godoy, I.J.; Santos, J.F.; Doyle, J.J.; Guimarães, P.M.; Abernathy, B.L.; Jackson, S.A.; Moretzsohn, M.C.; Bertioli, D.J. Segmental allopolyploidy in action: Increasing diversity through polyploid hybridization and homoeologous recombination. *Am. J. Bot.* **2018**, *105*, 1053–1066. [CrossRef] [PubMed]

93. Bertioli, D.J.; Seijo, G.; Freitas, F.O.; Valls, J.F.M.; Leal-Bertioli, S.C.M.; Moretzsohn, M.C. An overview of peanut and its wild relatives. *Plant Genet. Resour. Characterisation Util.* **2011**, *9*, 134–149. [CrossRef]

94. Galvão, L.S.; Roberts, D.A.; Formaggio, A.R.; Numata, I.; Breunig, F.M. View angle effects on the discrimination of soybean varieties and on the relationships between vegetation indices and yield using off-nadir Hyperion data. *Remote Sens. Environ.* **2009**, *113*, 846–856. [CrossRef]

95. Sakamoto, T.; Gitelson, A.A.; Wardlow, B.D.; Arkebauer, T.J.; Verma, S.B.; Suyker, A.E.; Shibayama, M. Application of day and night digital photographs for estimating maize biophysical characteristics. *Precis. Agric.* **2012**, *13*, 285–301. [CrossRef]

96. Perry, E.M.; Roberts, D.A. Sensitivity of narrow-band and broad-band indices for assessing nitrogen availability and water stress in an annual crop. *Agron. J.* **2008**, *100*, 1211–1219. [CrossRef]

97. Meng, J.; Xu, J.; You, X. Optimizing soybean harvest date using HJ-1 satellite imagery. *Precis. Agric.* **2015**, *16*, 164–179. [CrossRef]

98. Mullan, D. Spectral radiometry. In *Physiological Breeding: Interdisciplinary Approaches to Improve Crop Adaptation*; Reynolds, M., Pask, A., Mullan, D., Eds.; CIMMYT: Batan, Mexico, 2012; pp. 69–80.

99. Araus, J.; Casadesus, J.; Bort, J. Recent tools for the screening of physiological traits determining yield. In *Application of Physiology in Wheat Breeding*; Reynolds, M., Ortiz-Monasterio, J., McNab, A., Eds.; CIMMYT: Batan, Mexico, 2001; pp. 59–77.

100. Zarco-Tejada, P.J.; Morales, A.; Testi, L.; Villalobos, F.J. Spatio-temporal patterns of chlorophyll fluorescence and physiological and structural indices acquired from hyperspectral imagery as compared with carbon fluxes measured with eddy covariance. *Remote Sens. Environ.* **2013**, *133*, 102–115. [CrossRef]

101. Tossim, H.A.; Nguepjop, J.R.; Diatta, C.; Sambou, A.; Seye, M.; Sane, D.; Rami, J.F.; Fonceka, D. Assessment of 16 peanut (*Arachis hypogaea* L.) CSSLs derived from an interspecific cross for yield and yield component traits: QTL validation. *Agronomy* **2020**, *10*, 583. [CrossRef]

102. Guo, L.; Chen, J.; Cui, X.; Fan, B.; Lin, H. Application of ground penetrating radar for coarse root detection and quantification: A review. *Plant Soil* **2013**, *362*, 1–23. [CrossRef]

103. Butnor, J.R.; Samuelson, L.J.; Stokes, T.A.; Johnsen, K.H.; Anderson, P.H.; González-Benecke, C.A. Surface-based GPR underestimates below-stump root biomass. *Plant Soil* **2016**, *402*, 47–62. [CrossRef]

104. Yeung, S.W.; Yan, W.M.; Hau, C.H.B. Performance of ground penetrating radar in root detection and its application in root diameter estimation under controlled conditions. *Sci. China Earth Sci.* **2015**, *59*, 145–155. [CrossRef]

105. Hirano, Y.; Dannoura, M.; Aono, K.; Igarashi, T.; Ishii, M.; Yamase, K.; Makita, N.; Kanazawa, Y. Limiting factors in the detection of tree roots using ground-penetrating radar. *Plant Soil* **2008**, *319*, 15–24. [CrossRef]

106. Pauli, D.; Chapman, S.C.; Bart, R.; Topp, C.N.; Lawrence-Dill, C.J.; Poland, J.; Gore, M.A. The quest for understanding phenotypic variation via integrated approaches in the field environment. *Plant Physiol.* **2016**, *172*, 622–634. [CrossRef]

107. Liu, X.; Dong, X.; Leskovar, D.I. Ground penetrating radar for underground sensing in agriculture: A review. *Int. Agrophys.* **2016**, *30*, 533–543. [CrossRef]